# The Effect of Submeso Motions on the Budgets of the Mean Turbulent Kinetic Energy and Temperature Variance in the Stable Atmospheric Surface Layer

**Mario Schiavon** ( mario.skiavon@gmail.com )
**Francesco Tampieri**
National Research Council
**Matteo Caggio**
Czech Academy of Sciences
**Mauro Mazzola**
National Research Council
**Angelo Pietro Viola**
National Research Council

**Research Article**

**Keywords:** Stable surface layer, Submeso motions, Temperature variance, Turbulent kinetic energy, Second-moment budgets

**Posted Date:** September 9th, 2022

**DOI:** https://doi.org/10.21203/rs.3.rs-2033615/v1

# The Effect of Submeso Motions on the Budgets of the Mean Turbulent Kinetic Energy and Temperature Variance in the Stable Atmospheric Surface Layer

**Mario Schiavon · Francesco Tampieri · Matteo Caggio · Mauro Mazzola · Angelo Pietro Viola**

Received: DD Month YEAR / Accepted: DD Month YEAR

**Abstract**
By considering turbulence observations in the atmospheric stable surface layer over complex terrain, we study the effect of submeso motions on the budgets of the mean turbulent kinetic energy (TKE) and (half) the temperature variance. Different averaging times are considered (i.e., 100 s and 30 min), to filter out or retain the submeso contributions to second-order moments. Furthermore, results are interpreted by introducing four parameters that express the relative submeso contribution to the TKE, the temperature variance, and the vertical fluxes of heat and momentum. Four regimes are identified according to these four submeso parameters and the budgets are evaluated for these regimes. A balance among production, buoyancy (for the TKE) and dissipation occurs for the two regimes characterized by small submeso contribution to the fluxes; whilst an unbalance occurs for the other two regimes, where the submeso contribution to the fluxes is large. Instead, the budgets are independent of the magnitude of the submeso contribution to the TKE and the temperature variance.

M. Schiavon
Independent
E-mail: mario.skiavon@gmail.com

F. Tampieri
National Research Council, Institute of Atmospheric Sciences and Climate (CNR-ISAC), Via P. Gobetti 101, 40129, Bologna, Italy

M. Caggio
Institute of Mathematics of the Academy of Sciences of the Czech Republic, Zitná 25, 11567, Praha 1, Czech Republic

M. Mazzola
National Research Council, Institute of Polar Sciences (CNR-ISP), Via P. Gobetti 101, 40129, Bologna, Italy

A. P. Viola
National Research Council, Institute of Polar Sciences (CNR-ISP), Via Fosso del Cavaliere 100, 00133, Roma, Italy

**Keywords** Stable surface layer · Submeso motions · Temperature variance · Turbulent kinetic energy · Second-moment budgets

## 1 Introduction

The understanding and modelling of the atmospheric stable boundary layer (SBL) is complicated by the coexistence of motions on a wide range of scales, from eddies close to the Kolmogorov scale to submeso motions. Following Mahrt (2014), we consider submeso motions as "motions between the main turbulent eddies and smallest mesoscale motions, traditionally specified to be 2 km horizontal scale" although a clear scale separation is not always observed. Being related to many physical phenomena (Mahrt 2007), these motions are ubiquitous and characterize a wide range of atmospheric flows. In presence of them, velocity and temperature spectra, and fluxes (co)spectra, are characterized by non negligible amplitudes at low frequencies (Acevedo et al. 2014; Schiavon et al. 2019; Mortarini and Anfossi 2015).

Several studies showed the limitations of the conventional paradigms (such as Monin-Obukhov similarity theory) in the description of turbulence in the SBL. These limitations were related to different "regimes" of the atmospheric flow, defined according to several parameters, such as stability (Grachev et al. 2013), wind speed (Sun et al. 2012, 2016; Van de Wiel et al. 2012; Mahrt et al. 2013, 2015; Acevedo et al. 2016), turbulence anisotropy (Mortarini et al. 2019; Stiperski and Calaf 2018; Stiperski et al. 2019) and the stength of submeso motions (Acevedo et al. 2014).

Another issue of the SBL is the the choice of the averaging time over which second-order moments are calculated (Vickers and Mahrt 2003, 2006; Howell and Sun 1999; Falocchi et al. 2019). Indeed, this choice is particularly difficult in presence of submeso motions and may affect the convergence of time averages to ensemble averages, which is a key assumption for the applicability of Reynolds-averaged equations.

This study deals with the Reynolds averaged equations for the mean turbulent kinetic energy (TKE) and (half) the temperature variance, to investigate the role of submeso motions on the assumptions necessary for closing the equations, with the analysis focusing on near-neutral and stable conditions. Except for the convergence of time averages to ensemble averages, the validity of these equations is independent on the spectral features of the concerned variables and thus of the presence of submeso motions. However, submeso motions may affect the closures or the driving terms in the budget. For instance, velocity-, length- and temperature-scales may change, or extra terms have to be considered in the parametrizations.

The paper is organized as follows. Observations and data analysis are described in Sect. 2. Section 3 introduces the submeso parameters used in this study, presents the budgets of the TKE and half the temperature variance, and discusses the regime classification of the data. In Sect. 4, the relation between submeso parameters and spectra is discussed. Results are presented in Sect. 5 and Sect. 6 summarizes the conclusions.

## 2 Observations and Data Analysis

Capital and tiny letters represent mean quantities and their turbulent fluctuations, respectively, while angle brackets denote time averaging: $U$ is the mean wind speed (vectorial average); $u$, $v$, and $w$ are the turbulent fluctuations of the stream-wise, crosswind, and vertical velocity components, respectively; $\Theta$ is the mean potential temperature and $\theta$ its turbulent fluctuation.

### 2.1 Site and Instrumentation

The investigation is based on the Climate Change Tower Integrated Project (CCT-IP) dataset (Mazzola et al. 2016b). In particular, two years (2012–2013) of observations at the Climate Change Tower (CCT) are considered in this study. The CCT is 34 m high and equipped with fast- and slow-response instruments at several levels: mean velocity, temperature and humidity are measured with slow-response instruments at 2, 4.8, 10.3, and 33.4 m above the ground, whilst three sonic anemometers are placed at intermediate levels: 3.7, 7.5 and 20.5 m (two Gill and one CSAT3, respectively). This study focuses on turbulence observation at the 7.5 m level, because, for technical reasons, few data are available from the other two levels during the considered period.

The experimental site is located in Ny-Ålesund (78°55′ N,11°55′ E), Svalbard, Norway, on the coast of Kongsfjorden, in an area with complex topography. The CCT is placed on a small relief (with height $\approx 50$ m asl and horizontal scale $\approx 500$ m), 2 km west to the Ny-Ålesund village and 1 km west to the Zeppelin mountain. Snow cover last from October to May whilst during the snow-free season, the ground is covered by stones and short grass, typical of arctic tundra. The roughness length is $z_0 \approx 10^{-4}$–$10^{-3}$ m for snow-free surface and $z_0 \approx 10^{-5}$–$10^{-4}$ m for snow-covered surface, depending on wind direction (Schiavon et al. 2019). In this study, both snow-free and snow-covered conditions are considered without any distinction, because results do not differ for the two cases.

### 2.2 Data Processing

Raw data were divided in 30 min records. Sonic data, recorded at 20 Hz, were checked for spikes, plausibility limits and gaps. A double rotation is used to align the sonic reference system to the 30 min mean velocity. Records with flow through the tower, $\Delta U/\Delta z < 0$ in the layer $2 - 10.3$ m or positive fluxes of heat and momentum (i.e., $uw$ and $w\theta$) calculated as 30-min covariances were discarded.

First-order moments ($U$ and $\Theta$) were calculated as 30-min averages. Stable conditions are selected by imposing positive bulk Richardson number, $R_\mathrm{B}$. By definition (e.g., Tampieri 2017):

$$R_B \equiv \frac{(z_2 - z_1)\beta \Delta\Theta(z_1, z_2)}{\Delta U^2(z_1, z_2)} \tag{1}$$

where $U$ and $\Theta$ are measured by slow-response instruments at $z_1 = 2\,\mathrm{m}$ and $z_2 = 10.3\,\mathrm{m}$ (i.e., below and above the level of turbulence observations, $z = 7.5\,\mathrm{m}$).

Vertical gradients of mean wind speed and temperature, which enters in the production terms of the budgets (Sect. 3), were estimated as finite differences between slow-response observations at $z_1 = 2\,\mathrm{m}$ and $z_2 = 10.3\,\mathrm{m}$ (but similar results were obtained by fitting all slow-response observations with a log-log[2] profile and then calculating the derivative at the sonic level).

To account for the submeso motions, second-order moments were calculated in two ways:

- full-scale (co)variances, calculated over the whole record length, i.e., 30 min;
- small-scale (co)variances, calculated by integrating 30-min multiresolution decomposition (MRD) (co)spectra (Howell and Mahrt 1997; Howell and Sun 1999; Vickers and Mahrt 2003) from the smallest time scale up to a cut-off time $T$ – this corresponds to divide the 30-min record in non overlapping sub-records of duration $T$, calculate the (co)variance over each sub-record and then average over all the sub-records referring to the 30-min interval.

Because a spectral gap is generally not observed in this data set, the cut-off time $T$ was chosen by considering the peak time-scale of the $uw$, $w\theta$, and $w^2$ MRD (co)spectra, i.e., the time scale for which the MRD (co)spectrum has its maximum. Figure 1 shows the distribution of this time scale for the three (co)spectra (in stable conditions). Grey areas correspond to the expected variability range in case of no submeso contribution and are estimated from Kaimal et al. (1972, their Fig.s 18 and 19), that found $0.1 \lesssim f_{uw} \lesssim 1.0$, $0.2 \lesssim f_{w\theta} \lesssim 1.0$, and $0.5 \lesssim f_{w^2} \lesssim 2$, for the peak frequency of the $uw$, $w\theta$, and $w^2$ (co)spectra respectively. The non-dimensional frequency $f \equiv nz/U$ (with $n$ in Hz) was transformed into the MRD time scale by taking $n \sim T^{-1}$, $z = 7.5\,\mathrm{m}$, $0.5\,\mathrm{m\,s^{-1}} < U < 10\,\mathrm{m\,s^{-1}}$ and by assuming that a broad relationship exists between MRD and Fourier spectra (Vickers and Mahrt 2003).

As expected, the $w^2$ spectra always peak in the small scale range (Fig. 1c), because, close to the ground, submeso motions cannot contribute to vertical velocity fluctuations (Højstrup 1982). Instead, bimodal distributions are observed for $T_{uw}$ and $T_{w\theta}$ (Fig. 1a,b): small and large submeso contribution corresponds to $uw$ and $w\theta$ cospectra peaking in the small-scale (grey area) and large-scale range, respectively. Thus $T = 100\,\mathrm{s}$ is chosen for the cut-off time, because it falls in the gap of these distributions and it is larger than most of the $w^2$ peak times (Fig. 1c).

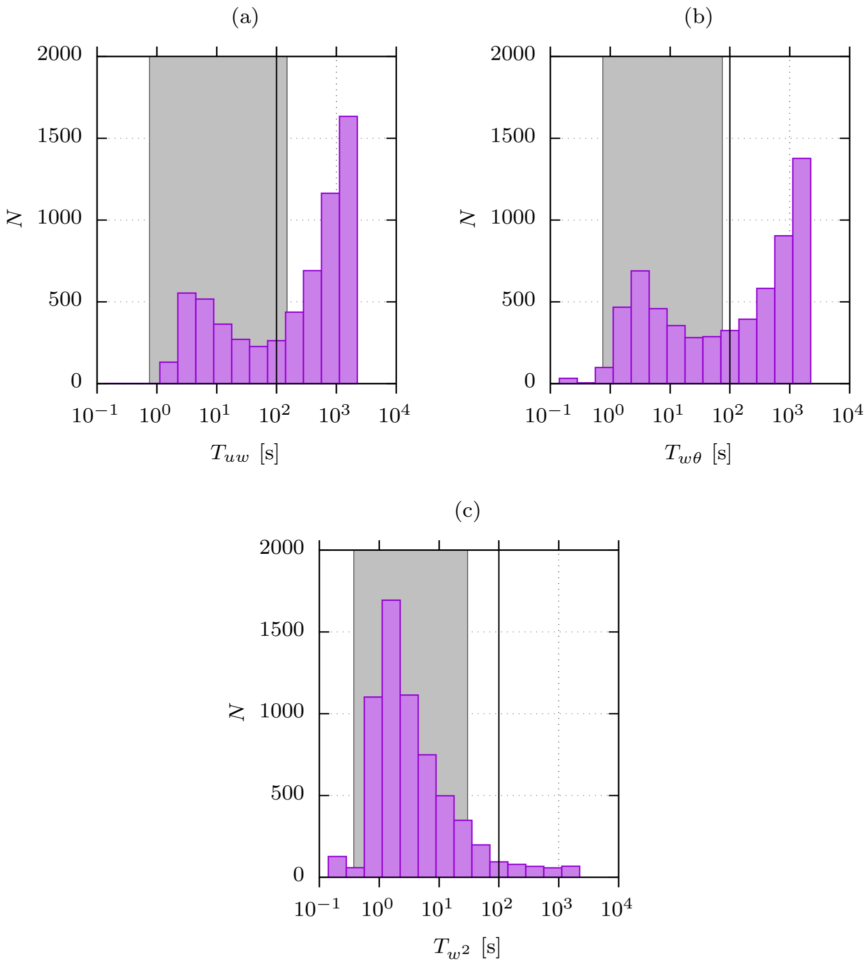


**Fig. 1** Distribution of the peak time (in s) of the (a) $uw$, (b) $w\theta$, and (c) $w^2$ MRD (co)spectra: $N$ is the number of spectra falling in a given peak-time interval (on a logarithmic scale). The grey area is an estimation of the expected variability range for no submeso contribution (see text). The chosen cut-off time, 100 s, is also shown

Hereinafter, the full-scale and small-scale (co)variances are indicated with the subscript 30 min and 100 s, respectively: eg., $\langle uw \rangle_{30\text{min}}$ and $\langle uw \rangle_{100\text{s}}$ are the full-scale and the small-scale momentum flux.

Fourier spectra calculated over each 30-min record are used to estimate the TKE and $\langle \theta^2 \rangle/2$ dissipation rate. In particular, the TKE dissipation rate is obtained from the inertial subrange of the $u^2$, $v^2$, and $w^2$ spectra as

$$\epsilon_x = \frac{2\pi}{U}\sqrt{\left(\frac{S_x(n) n^{5/3}}{\alpha_x}\right)^{3/2}} \qquad (2)$$

where $x = u, v, w$ represents velocity component, $S_x(n)$ is the value of the frequency $n$ (in Hz), $\alpha_u = 0.55$, $\alpha_{v,w} = (4/3)\alpha_u$, and the overline is frequency averaging over the interval $U/z < n < 4\,\mathrm{Hz}$ for $x = u$, and $2U/z < n < 4\,\mathrm{Hz}$ for $x = v, w$. The lower boundary of the averaging interval roughly corresponds the low-frequency end of the inertial subrange (e.g. Kaimal and Finnigan 1994), while $n < 4\,\mathrm{Hz}$ avoids aliasing effects.

It results that $\epsilon_u$ is $\approx 10\%$ larger than $\epsilon_v \simeq \epsilon_w$. This is however consistent with inertial subrange isotropy (Yadav et al. 1996). Thus, the mean among the three velocity components, $\epsilon \equiv (\epsilon_u + \epsilon_v + \epsilon_w)/3$, is taken as the estimate for the TKE dissipation rate.

Similarly, the half the temperature variance dissipation rate is obtained from the inertial subrange of the $\theta^2$ spectrum:

$$\epsilon_\theta = \frac{\epsilon^{1/3}\overline{S_\theta(n)n^{5/3}}}{\beta_1}\left(\frac{2\pi}{U}\right)^{2/3} \tag{3}$$

where $\beta_1 = 0.8$ (Kaimal et al. 1972) and the overline indicates averaging over the frequency range $U/z < n < 4\,\mathrm{Hz}$.

The estimation of the dissipation rates from velocity and temperature spectra limits the maximum wind speed of the considered dataset, which is $U \approx 10\,\mathrm{m\,s^{-1}}$ at 7.5 m. Indeed, for $U \gtrsim 10\,\mathrm{m\,s^{-1}}$, the sampled inertial subrange is too short for a reliable estimation of $\epsilon$ and $\epsilon_\theta$.

## 3 TKE and Temperature Variance Budgets in Presence of Submeso Motions

The budgets of the TKE and half the temperaure variance are presented by considering the effect of the submeso motions through the definition of four submeso parameters.

### 3.1 Definition of the Submeso Parameters

To quantify the strength of the submeso effect, the following parameter is defined

$$R_\xi \equiv \frac{\langle\xi\rangle_{30\mathrm{min}}}{\langle\xi\rangle_{100\mathrm{s}}} - 1, \tag{4}$$

which expresses the relative low-frequency contribution to the (co)variance $\xi$: $\langle\xi\rangle_{30\mathrm{min}}$ is the full-scale (co)variance and $\langle\xi\rangle_{100\mathrm{s}}$, the small-scale (co)variance. Thus $|R_\xi| \ll 1$ and $\gtrsim 1$ broadly corresponds to small and large submeso effect, respectively.

In the similar attempt to quantify the submeso effect, other authors used similar parameters. Acevedo et al. (2014) quantified the importance of submeso motions by using the ratio among the submeso TKE and the vertical velocity variance. Mahrt (2007, Eq. 10) considered the submeso effect on the shear stress vector. The stationarity index proposed by Foken and Wichura (1996),

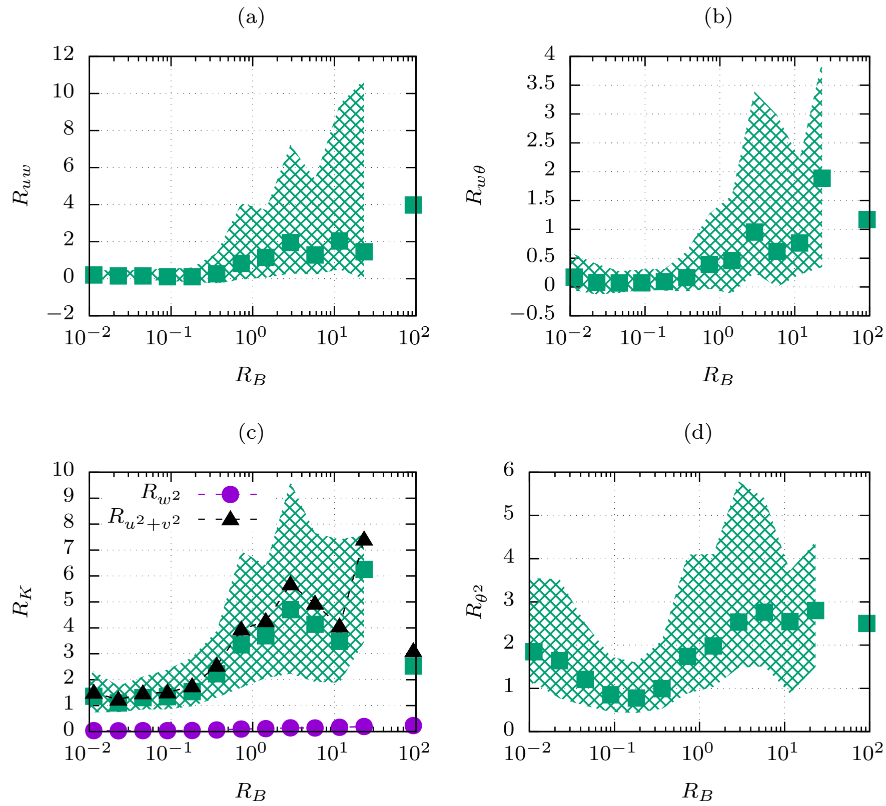


**Fig. 2** The four submeso parameters considered in this study as function of $R_B$: (a) $R_{uw}$, (b) $R_{w\theta}$, (c) $R_K$, and (d) $R_{\theta^2}$. Data are binned in intervals of $R_B$: median values, points, and 25th-75th percentile range (dashed area) are shown. In plot (c), median values of $R_{u^2+v^2}$ (black triangles) and $R_{w^2}$ (purple dots) are also shown

which quantifies the relative contribution to second-order moments from time scales close to the averaging time, is closely related to Eq. (4).

Focusing on the TKE and the temperature variance budgets (Sects. 3.2 and 3.3), four submeso parameters are considered: $R_K$, with $K \equiv (u^2+v^2+w^2)/2$, related to the TKE; $R_{\theta^2}$, related to the potential temperature variance; $R_{uw}$ and $R_{w\theta}$, related to the vertical fluxes of momentum and heat, respectively.

Altough the submeso parameters are not directly related to the stability, the influence of submeso motions increases under more stable conditions (Mahrt 2014). Figure 2 shows the four sumeso parameters considered in this study against $R_B$ (data are binned in $R_B$). Overall, at least for $R_B \gtrsim 0.5$, the main effect of increasing $R_B$ is to augment the variability of the sumeso parameters (dashed area). In the same stability interval, median values also increase especially for $R_K$ and $R_{\theta^2}$ (Figs. 2c,d) whilst their variation is smaller for $R_{uw}$ and $R_{w\theta}$: as expected, and confirmed in Sect. 4, the submeso contribution to the variances is more systematic than in covariances. The increase of $R_K$, both in median and variability, is due to the horizontal velocity components, having $R_K \approx R_{u^2+v^2} \gg R_{w^2}$ over the whole stability range (Fig. 2c).

Approaching near-neutral conditions, $R_B \lesssim 0.5$, the submeso parameters become almost independent of $R_B$, with little variability, if $R_{uw}$, $R_{w\theta}$, and $R_K$ are considered (Fig. 2a,b,c). The different behaviour of $R_{\theta^2}$, which increases both in median values and variability as $R_B \to 0$, is likely related to low-frequency temperature fluctuations triggered by surface heterogeneity.

### 3.2 Turbulent Kinetic Energy Budget

Assuming horizontal homogeneity and $dV/dz = 0$, the budget equation for the mean turbulent kinetic energy, $\langle K \rangle = (\langle u^2 \rangle + \langle v^2 \rangle + \langle w^2 \rangle)/2$, reads

$$T_K = P + B - \epsilon, \tag{5}$$

where

$$P = -\langle uw \rangle \frac{dU}{dz} \tag{6}$$

is shear production,

$$B = \beta \langle w\theta \rangle, \tag{7}$$

is buoyancy (with $\beta = g/\Theta_0$),

$$T_K = \frac{d\langle K \rangle}{dt} + \frac{d}{dz} \left\langle \frac{u_i u_i w}{2} + pw \right\rangle. \tag{8}$$

is the time derivative of the TKE and the vertical divergence of the third-order moments, and $\epsilon$ is the viscous dissipation rate.

Theoretically, the budget is satisfied for ensemble averages. In practice, we use time averages (over 30 min and 100 s). If the averaging time is long enough to give a fair approximation of the ensemble average, the budget based on observations is closed. Otherwise, an unbalance is expected due to the presence of modes not included in the average. Assuming that 30-min is long enough to have statistical convergence, Eq. 5 is the budget for 30-min averages, i.e., full-scale turbulence:

$$T_{K,30\text{min}} = P_{30\text{min}} + B_{30\text{min}} - \epsilon. \tag{9}$$

If the full-scale fluxes in shear production and buoyancy of Eq. 9 are expressed in terms of the small-scale fluxes and the corresponding submeso parameters, we have:

$$T_{K,30\text{min}} = P_{100s} + B_{100s} + [R_{uw} P_{100s} + R_{w\theta} B_{100s}] - \epsilon. \tag{10}$$

The term in square brackets evidences that, even in the stationary and vertically homogeneous case ($T_{K,30\text{min}} = 0$), the budget is not satisfied for the small-scale turbulence if submeso motions are effective, i.e., if the submeso parameters $R_{uw}$ and $R_{w\theta}$ are significantly different from zero. In the same conditions, the budget does not involve the absolute value of $\langle K \rangle$, because it expresses equilibrium among shear production, buoyancy loss, and dissipation. Thus the TKE submeso parameter, $R_K$, is expected to have a minor influence on the budget, possibly limited to the cases where transport and unsteadiness are important, i.e. when $T_{K,30\text{min}}$ is not negligible.

### 3.3 Temperature Variance Budget

Under the same assumptions of the TKE budget, the budget for half the variance of the potential temperature reads

$$T_\theta = P_\theta - \epsilon_\theta, \tag{11}$$

where

$$P_\theta = -\langle w\theta \rangle \frac{d\Theta}{dz} \tag{12}$$

is gradient production,

$$T_\theta = \frac{1}{2}\left(\frac{d\langle \theta^2 \rangle}{dt} + \frac{d\langle w\theta^2 \rangle}{dz}\right) \tag{13}$$

is the time derivative of the variance and the vertical divergence of the third-order moments, and $\epsilon_\theta$ is the viscous dissipation rate.

As for the TKE budget, we can assume that Eq. 11 represents the budget for full-scale turbulence (30-min averages),

$$T_{\theta,30\text{min}} = P_{\theta,30\text{min}} - \epsilon_\theta, \tag{14}$$

which can be expressed in terms of small-scale turbulence by using the heat flux submeso parameter, $R_{w\theta}$,

$$T_{\theta,30\text{min}} = P_{\theta,100s} + [R_{w\theta} P_{\theta,100s}] - \epsilon_\theta, \tag{15}$$

As for the TKE budget (Eq. 10), the term in square brackets highlights the effect of the submeso motion and the role of the temperature variance submeso parameter, $R_{\theta^2}$, if any, is expected to be limited to the case when unsteadiness is important (i.e., when $T_{\theta,30\text{min}}$ is not negligible).

### 3.4 Regimes

To understand the effect of submeso motions on the budgets, a broad classification is formulated, according to the values of the corresponding submeso parameters.

Figure 3 shows the data distribution in the plane $[R_{uw} + R_{w\theta}, R_K]$ and $[R_{w\theta}, R_{\theta^2}]$ – which are relevant for the TKE and the temperature variance budget, respectively – for all the stability range, weak stability ($R_B < 0.05$) and large stability ($R_B > 0.5$). For convenience, $R_{uw} + R_{w\theta}$ is considered for

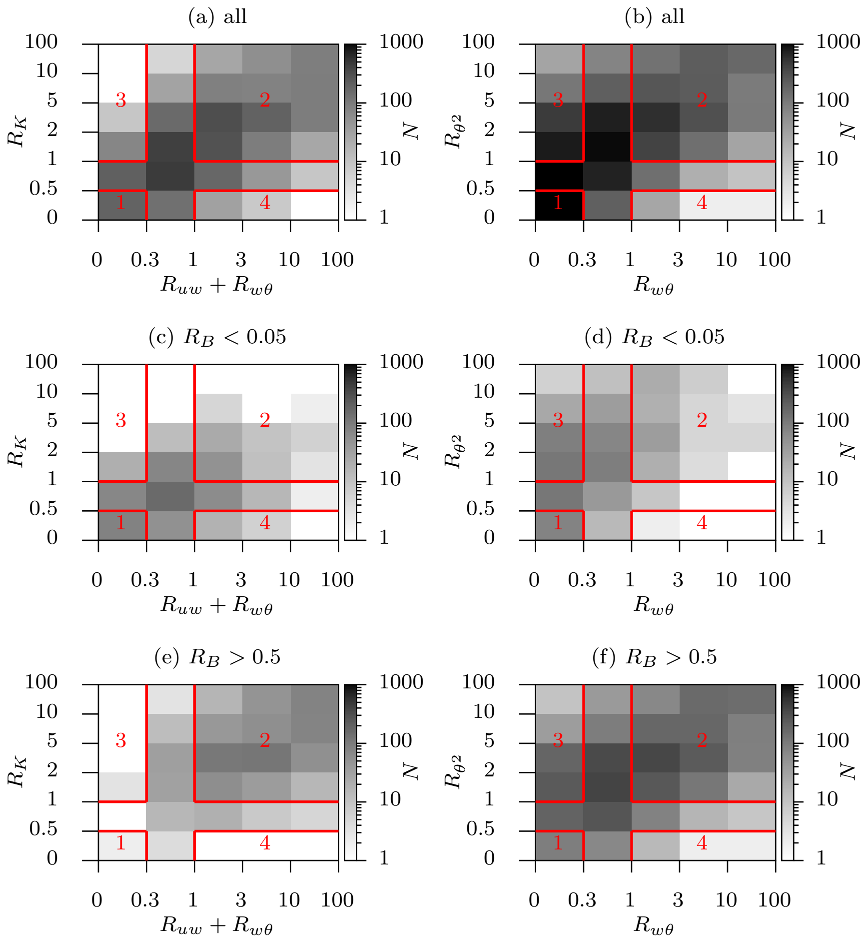


**Fig. 3** Data distribution in the $[R_{uw} + R_{w\theta}, R_K]$ plane (a,c,e) and in the $[R_{w\theta}, R_{\theta^2}]$ plane (b,d,f), for the whole stability range (a,b), $R_B < 0.05$ (c,d), and $R_B > 0.5$ (e,f). Colors represent, on a logarithmic scale, the number of 30-min records falling in each rectangle (the scale of the axes is not uniform). The regions corresponding to the four regimes used in this study are also indicated (red lines and numbers)

the TKE budget, instead of the two parameters separately: note that both parameters are usually positive for this dataset (Fig. 2a,b). However, presented results are independent of this choice. Consistently with Fig. 2, and especially for the submeso parameters related to the TKE budget (Fig. 2a,c,e), data corresponding to weakly stable conditions (and strong winds) are more concentrated in the region with small submeso parameters ($R_\xi < 1$, Fig. 2c), whilst more stable conditions (and weak winds) corresponds to large submeso parameters ($R_\xi > 1$, Fig. 3e).

**Table 1** The thresholds for the submeso parameters used for the four-regime classification of the data, for the TKE and half the temperature variance budget

| Regime | $\langle K \rangle$ budget | $\langle \theta \rangle^2/2$ budget |
|---|---|---|
| 1 | $R_{uw} + R_{w\theta} < 0.3$ and $R_K < 0.5$ | $R_{w\theta} < 0.3$ and $R_{\theta 2} < 0.5$ |
| 2 | $R_{uw} + R_{w\theta} > 1$ and $R_K > 1$ | $R_{w\theta} > 1$ and $R_{\theta 2} > 1$ |
| 3 | $R_{uw} + R_{w\theta} < 0.3$ and $R_K > 1$ | $R_{w\theta} < 0.3$ and $R_{\theta 2} > 1$ |
| 4 | $R_{uw} + R_{w\theta} > 1$ and $R_K < 0.5$ | $R_{w\theta} > 1$ and $R_{\theta 2} < 0.5$ |

To study the submeso effect on the TKE and temperature variance budgets, data are classified in four regimes:

- Regime 1: $R_K \ll 1$ and $R_{uw} + R_{w\theta} \ll 1$ for the TKE; $R_{\theta^2} \ll 1$ and $R_{w\theta} \ll 1$ for the temperature variance. In this regime, there is negligible submeso forcing on the budgets and the time average is expected to give a fair approximation of the ensemble average. Budgets for 30 min and 100 s are expected to be similar.
- Regime 2: $R_K > 1$ and $R_\tau + R_{w\theta} > 1$ for the TKE; $R_{\theta^2} > 1$ and $R_{w\theta} > 1$ for the temperature variance. In this regime, submeso motions contribuite both to the variances and the fluxes, thus affecting production/loss terms (Eqs.(10) and (15)) and, possibly, unsteadiness and third-order terms. The budgets for 30 min and 100 s are expected to differ.
- Regime 3: $R_\tau + R_{w\theta} \ll 1$ and $R_K > 1$ for the TKE; $R_{w\theta} \ll 1$ and $R_{\theta^2} > 1$ for the temperature variance. In this regime the submeso motions affect the variances but not the fluxes (and thus the production/buoyancy terms in the budget). Considering the budgets, this regime is thus similar to regime 1, while, as regime 2, it is relevant when the share between horizontal and vertical velocity variances are considered.
- Regime 4: $R_{uw} + R_{w\theta} > 1$ and $R_K \ll 1$ for the TKE budget; $R_{w\theta} > 1$ and $R_{\theta^2} \ll 1$ for the temperature variance. In this regime, a submeso effect is expected on the budgets but not on the variances.

To cope with this four-regime classification and have a significant number of observations for each regime, the thresholds reported in Tab. 1 are used in this study. These thresholds and the regions corresponding to the four regimes are indicated in Fig. 3.

## 4 Relation Between Submeso Parameters and Spectra

Because submeso parameters reflect the spectral distribution of second-order moments, that may affect the budgets (for instance by determining the convergence of time averages), velocity, temperature and fluxes (co)spectra are presented in this section, for different values of submeso parameters.

Figure 4 shows the spectral distribution of the horizontal and vertical velocity variance, the temperature variance, and the fluxes of heat and momentum, for a given interval of $R_B$ and the four submeso regimes discussed in Sect. 3.4.

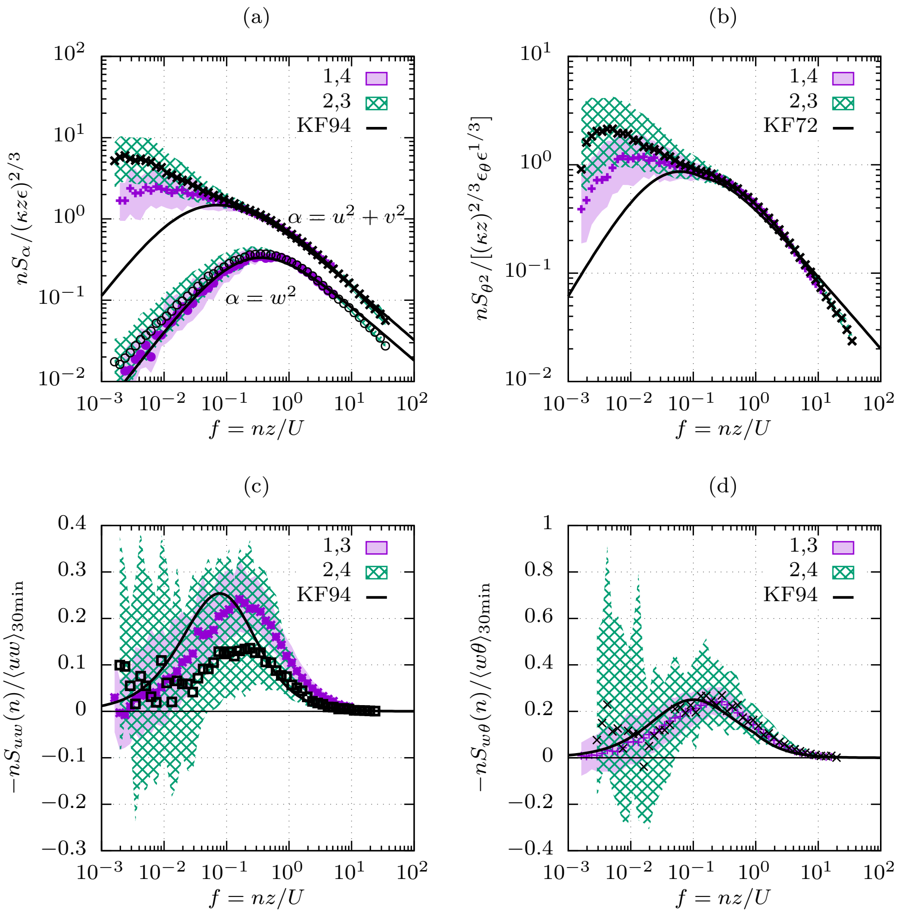


**Fig. 4** Observed spectra for different submeso regimes (indicated by numbers) and $0.1 < R_B < 0.2$: (a) horizontal and vertical velocity components; (b) temperature; (c) momentum flux; (d) heat flux. Velocity and temperature spectra are normalized in the inertial subrange, whilst flux cospectra are normalized with the full-scale flux. For each statistic, spectra belonging two different regimes associated with the same threshold of the relative submeso parameter are combined (see text). Median values (points) and variability (25th-75th percentile range, dashed area) are shown along with spectral models from Kaimal and Finnigan (1994) (KF94) and Kaimal et al. (1972) (KF92)

In particular, velocity and momentum-flux (co)spectra are separated according to TKE regimes (Fig. 4a,c), whilst temperature and heat-flux (co)spectra are separated according to the temperature-variance regimes (Fig. 4b,d). Furthermore, regimes corresponding to the same threshold of the relevant submeso parameter for that spectrum are combined. For instance, for the velocity spectra, whose relevant parameter is $R_K$, regimes 1,4 and 2,3 are combined (Fig. 4a), because they are related to same threshold of $R_K$, i.e., $R_K < 0.5$ and $> 1$, respectively (Tab. 1). Whilst regimes 1,3 and 2,4 are combined for the momentum flux cospectra (Fig. 4c), whose relevant parameter is $R_{uw}$. Although only one interval of $R_B$ is presented, similar results are observed for different stability.

Velocity and temperature spectra are normalized in the inertial subrange, whilst flux cospectra are normalized with the full-scale flux. For comparison, spectral models from Kaimal and Finnigan (1994) and Kaimal et al. (1972) are also shown, because they are proper for a boundary layer without submeso motions.

The submeso contribution is evident in the low-frequency range ($f < 0.1$) of the horizontal-velocity and temperature spectra (Fig. 4a,b) and, as expected, its relative magnitude increases from regimes 1,4 to 2,3. Instead, the $w^2$ spectrum does not show any submeso contribution, independently of the submeso regime, because large-scale vertical velocity fluctuations are damped close to the ground.

As noted in Sect. 2, no spectral gap is present in the $u^2 + v^2$ and $\theta^2$ spectra. Furthermore, because $u^2 + v^2$ spectra level off or even increase with decreasing $f$ (Fig. 4a), statistical convergence is not expected for the horizontal velocity variance even when 30 min averages are considered. Independently of the submeso contribution, a clear inertial subrange is present for all velocity components and temperature.

Figures 4c and d show the cospectra of the momentum and the heat flux, respectively. The behaviour of the two cospectra is similar. For regimes 1,3, for which the submeso contribution to the flux is small, observed cospectra are close to Kaimal and Finnigan (1994) spectral models, whilst the normalization by full-scale co-variances lowers the average spectral levels for regimes 2,4, for which the submeso contribution is large. As observed by other authors (Vickers and Mahrt 2003), the submeso contribution to the fluxes is highly variable, both in magnitude and sign, thus resulting less systematic than in velocity and temperature spectra.

## 5 Results

The TKE and half the temperature variance budget presented in Sect. 3 are evaluated from observations by considering both full-scale and small-scale (co)variances and separating the data in the four submeso regimes discussed in Sect. 3.4.

### 5.1 The TKE Budget

By using observations, we can directly evaluate production, $P$, buoyancy, $B$, and dissipation, $\epsilon$, whilst the combination of unsteadiness and third order terms, i.e., $T_K$, is taken as the residual of the former terms.

Fig. 5a shows $(P_{30\mathrm{min}} + B_{30\mathrm{min}})/\epsilon$ (namely the production/loss normalized over the dissipation, which is equal to 1 in absence of vertical transport and

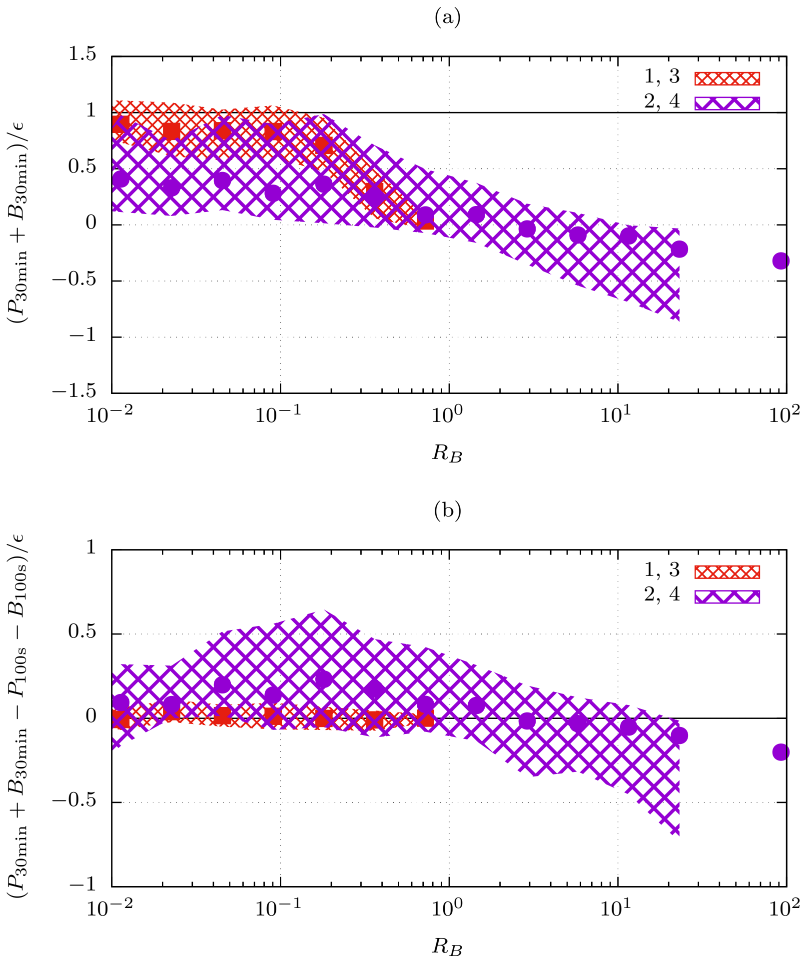


**Fig. 5** (a) Shear production plus buoyancy, $P_{30\text{min}} + B_{30\text{min}}$, evaluated for full-scale statistics (30 min), normalized with the dissipation rate, $\epsilon$, vs $R_B$, for the two pair of submeso regimes 1,3 and 2,4; data are binned in $R_B$: median values (points) and 25th-75th percentile range (dashed areas), are shown. (b) As in plot (a), but for the difference in $(P + B)/\epsilon$ between full-scale and small-scale (100 s) statistics

unsteadiness and if time averages represent ensemble averages) vs $R_B$, for the four regimes discussed in Sect. 3.4. Regimes 1 and 3, and 2 and 4, are considered together because they give similar results (not shown), thus confirming the minor role of $R_K$ in the TKE budget (Sect. 3.2). Figure 5b shows the difference in the production/loss term between full-scale (30 min) and small-scale (100 s) covariances, with the same regime classification used in Fig. 5a.

In regimes 1,3, a balance between shear production, buoyancy and dissipation occurs for $R_B \leq 0.2$, while an unbalance is observed for larger stability (Fig. 5a). As expected (Sect. 3.4), there is no difference between full-scale and

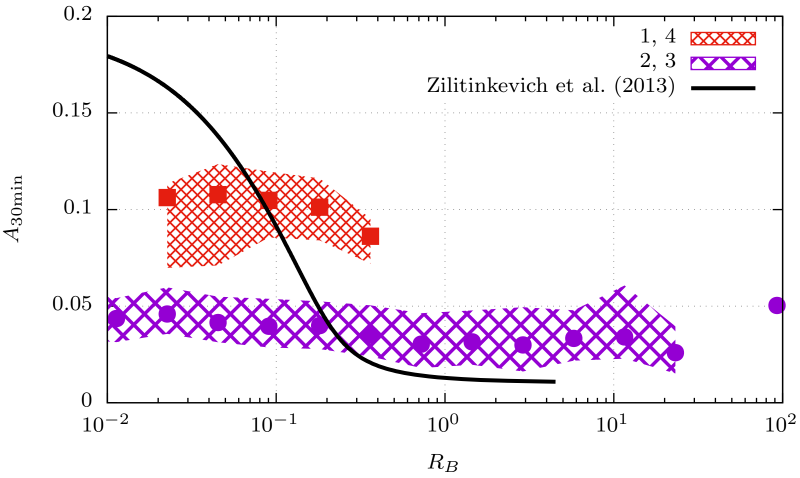


**Fig. 6** Full-scale turbulence anisotropy ratio $A_{30\mathrm{min}} = [\langle w^2\rangle/(\langle u^2\rangle + \langle v^2\rangle)]_{30\mathrm{min}}$ vs $R_B$ for the four TKE regimes, paired according to the threshold in $R_K$: i.e., 1,4 and 2,3. The relationship $A(Ri)$ from Zilitinkevich et al. (2013) is shown for comparison (by assuming $Ri \approx R_B$)

small-scale statistics (Fig. 5b), because full-scale and small-scale fluxes are equal. Most of the unbalance observed for $R_B \geq 0.2$, which corresponds to $T_{K,30\mathrm{min}} < 0$ and indicates that dissipation is larger than the sum of production and buoyancy ($(P+B)/\epsilon < 1$), may be related to the contribution of the divergence of third-order moments that acts as a source of TKE (Eq. (8)). Note that, for $R_B \approx 1$, $(P+B)/\epsilon \approx 0$ and thus $T_{K,30\mathrm{min}}/\epsilon \approx 1$: the balance is between transport and dissipation.

In regimes 2,4, $(P_{30\mathrm{min}} - B_{30\mathrm{min}})/\epsilon < 1$ for all the observed stability range, decreasing for increasing $R_B$, and becoming $< 0$ for $R_B > 1$ (Fig. 5a, purple area). This means that the maintenance of turbulence is due to the transport by third-order moments, i.e. $T_{K,30\mathrm{min}}$. As expected, the budget depends on the averaging time in these regimes, because the submeso contribution to the fluxes is significant, i.e., $R_{uw} + R_{w\theta} > 1$. On average, the unbalance is larger (because production is smaller) if small-scale turbulence is considered (Fig. 5b), but with a dependence on $R_B$. The unbalance among production, bouyancy and dissipation ($(P+B)/\epsilon < 1$ and $T_{K,30\mathrm{min}} < 0$), increasing with stability and observed also for 30-min averages, is consistent with transport of TKE from above, as occurs in an upside-down boundary layer (e.g., Mahrt and Vickers 2002; Mazzola et al. 2016a), and with the presence of submeso motions not included in the time averaging interval.

Although the role of $R_K$ on the TKE budget is negligible, this parameter is relevant in the statistics that involve the TKE itself. Figure 6 shows the stability dependence of the full-scale turbulence anisotropy ratio, i.e. $A_{30\mathrm{min}} = [\langle w\rangle^2/(\langle u\rangle^2 + \langle v\rangle^2)]_{30\mathrm{min}}$, for the four regimes of the TKE budget paired according to the common threshold in $R_K$ (1,4 and 2,3 for $R_K < 0.5$ and $> 1$, respectively). As expected, full-scale turbulence anisotropy decreases in the transition between regimes 1,4 and 2,3, from $A_{30\mathrm{min}} \approx 0.1$ to $\approx 0.05$. This is due to the two-dimensional nature of the submeso contribution, which affects $u^2$ and $v^2$ and not $w^2$ (Sec. 4), with a minor effect of stability. Furthermore, the fact that $A_{30\mathrm{min}} < 0.1$ for regimes 2,3, characterized by $R_K > 1$, is consistent with the criterion proposed by Mortarini et al. (2019) to individuate the presence of meandering motions.

Compared to full-scale turbulence, small-scale turbulence is characterized by a larger anisotropy ratio, i.e., $A_{100\mathrm{s}} \approx 0.15$, which is almost independent of stability and regime (not shown).

### 5.2 The Temperature Variance Budget

As for the TKE budget, the temperature variance budget is studied by evaluating gradient production, $P_\theta$, and dissipation, $\epsilon_\theta$.

Figure 7a shows $P_{\theta,30\mathrm{min}}/\epsilon_\theta$ vs $R_B$ for the four regimes discussed in Sect. 3.4. In particular, as for the TKE budget, data belonging to regimes 1,3 and 2,4 are considered together, because, as expected, results are independent of the submeso parameter related to the variance, $R_{\theta^2}$ (Sect. 3.3): the two paired regimes have the same threshold of $R_{w\theta}$, i.e. $R_{w\theta} < 0.3$ and $> 1$, respectively (Tab. 1).

For $R_B < 0.1$, dissipation exceeds production, $P_{\theta,30\mathrm{min}}/\epsilon_\theta < 1$, independently of the regime (Fig. 7a). As expected, $P_\theta \to 0$ as $R_B \to 0$, because $d\Theta/dz \to 0$ as neutral conditions are approached. Thus, the unbalance may be due to horizontal heterogeneity, which is not considered in Eq. 14, or by vertical transport, having $T_{\theta_{30\mathrm{min}}} < 0$. The fact that, contrary to vertical gradients and fluxes, $\langle\theta^2\rangle$ does not vanish approaching neutrality is a characteristic feature of the atmospheric surface-layer (e.g. Tampieri et al. 2009).

For $R_B > 1$, the temperature variance budget depends on the submeso regime and, in particular, on the relative submeso contribution to the heat flux, i.e., $R_{w\theta}$ (Fig. 7a). For regimes 1,3 ($R_{w\theta} < 0.3$), a balance between gradient production and dissipation occurs ($P_{\theta,30\mathrm{min}}/\epsilon_\theta = 1$, $T_{30\mathrm{min}} = 0$), with no difference between full-scale and small-scale turbulence, as expected (Fig. 7b). Instead, for regimes 2,4 ($R_{w\theta} > 1$), gradient production exceeds dissipation: $P_{\theta,30\mathrm{min}}/\epsilon_\theta \approx 2$, on average, but with large variability (Fig. 7a, purple area). This occurs especially for full-scale turbulence. Indeed, as for the TKE budget (Fig. 5b, purple area), production is larger for full-scale than for small-scale turbulence: $(P_{\theta,30\mathrm{min}} - P_{\theta,100\mathrm{s}})/\epsilon_\theta \approx 1$, on average (Fig. 7b, purple). In regimes 2,4 $P_{\theta,30\mathrm{min}}/\epsilon_\theta > 1$ and thus $T_{\theta,30\mathrm{min}} > 0$, meaning that third-order terms subtract variance from the budget.

## 6 Conclusions

Two years of turbulence observations in the stable atmospheric surface layer were considered to study the effect of the submeso motions on the TKE and

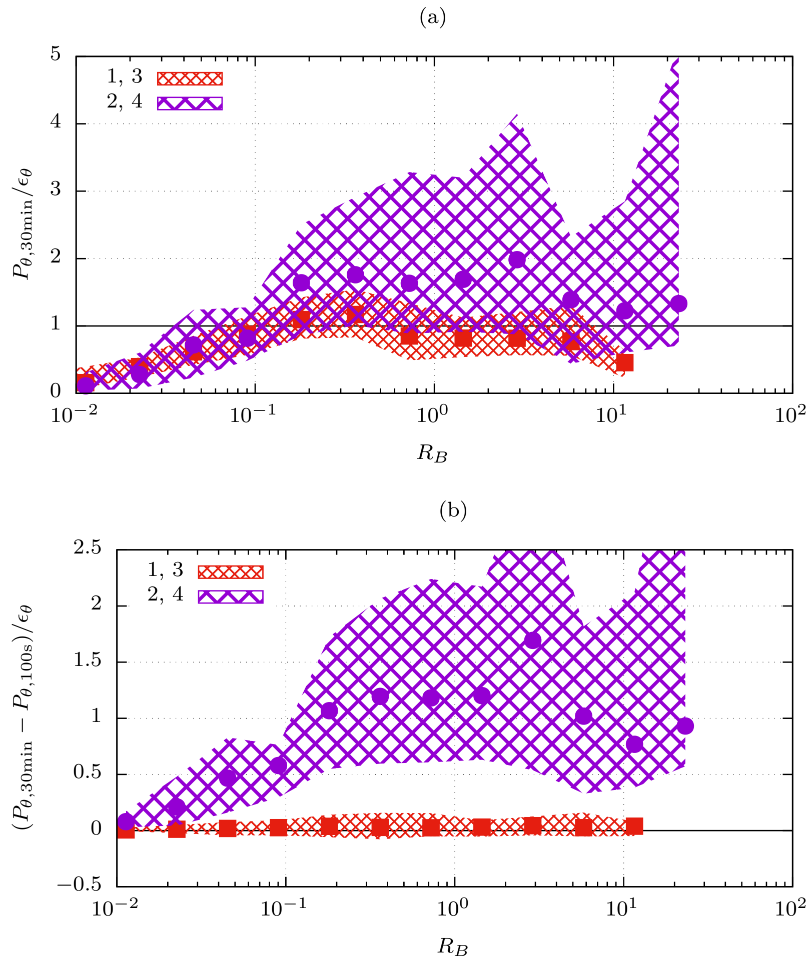


**Fig. 7** As in Fig. 5, but for the temperature-variance budget. (a) Gradient production over dissipation vs $R_B$ for full-scale turbulence, $P_{30\mathrm{min}}/\epsilon_\theta$, for the two pairs of sumeso regimes 1,3 and 2,4. (b) As in plot (a) but for the difference in $P_\theta/\epsilon_\theta$ between full-scale and small-scale turbulence

temperature variance budgets. To do this, the budgets were evaluated by using (co)variances calculated over two averaging times, i.e., 30 min and 100 s. Whilst submeso motions contribute to 30 min or "full-scale" (co)variances, the submeso contribution is largely filtered out in 100 s or "small-scale" (co)variances. Furthermore, four parameters were considered to quantify the relative submeso contribution to the TKE, the temperature variance, and the vertical fluxes of heat and momentum. Through them, the data were separated in four regimes:

– Regime 1, corresponding to small submeso contribution both to the TKE (or the temperature variance) and the fluxes;

– Regime 2, corresponding to large submeso contribution both to the TKE (or the temperature variance) and the fluxes;
– Regime 3, corresponding to large submeso contribution to the TKE (or the temperature variance) but small submeso contribution to the fluxes;
– Regime 4, corresponding to small submeso contribution to the TKE (or the temperature variance) but large submeso contribution to the fluxes.

For both the full-scale and the small-scale TKE and temperature variance budgets, a production-dissipation balance was observed for regime 1 and 3, up to moderate stability; whilst an unbalance occurred for regime 2 and 4 for the whole stability range. This indicates the important role in the budgets of the submeso contribution to the fluxes, which affects the production terms, and the negligible role of the submeso contribution to the variances.

Indeed, when the submeso contribution to the fluxes is not negligible, as in regimes 2 and 4, a term accounting for it, and depending on the submeso parameters, should be included in the budgets for small-scale turbulence. However, this term cannot explain all the observed unbalance, which occurs also in the full-scale budgets, that do not contain it. Part of this unexplained unbalance is probably related to effects or terms that could not be estimated in this study, such as transport by third-order moments, physically different states of the atmospheric surface-layer, and non-convergence of time averages to ensemble averages even for full-scale (co)variances (the latter being a major issue in presence of submeso motions). These results are related to those of other authors. In particular, considering the TKE budget, regimes 1,3 and 2,4 compare, respectively, with the unperturbed and perturbed surface-layer defined by Chamecki et al. (2018). Furthermore, although the submeso parameters related to the variances have no influence on the TKE and temperature-variance budgets, they are linked to the turbulence anisotropy degree, which is a key parameter in the characterization and modelling of the stable boundary layer (Zilitinkevich et al. 2013; Mortarini et al. 2019). Moreover, although the four regimes considered in this study do not superimpose exactly with the three limiting states of Stiperski and Calaf (2018), there are analogies about their relation to TKE budget, for instance, concerning the validity of the production-buoyancy-dissipation balance.

Objectives for future research are to verify the validity of this approach also for other datasets and better characterize the submeso contribution to the budgets, possibly parameterizing it.

## 7 Data Availability

The data generated and analysed in this study are available from the corresponding author with permission of the National Research Council, Institute of Polar Sciences (CNR-ISP).

## 8 Competing Interests

The authors have no competing interests to declare that are relevant to the content of this article.

## 9 Funding

M. C. has been supported by the Praemium Academiae of Š. Nečasová and by the Czech Science Foundation under the grant GAČR GA19-04243S.

**Acknowledgements** The authors thank the Department of Earth System Sciences and Technologies for the Environment of the National Research Council (CNR-DSSTTA) and its staff for the logistical support at the Arctic Station Dirigibile Italia in Ny-Ålesund.

## References

Acevedo OC, Costa FD, Oliveira PE, Puhales FS, Degrazia GA, Roberti D (2014) The influence of submeso processes on stable boundary layer similarity relationships. J Atmos Sci 71(1):207–225

Acevedo OC, Mahrt L, Puhales FS, Costa FD, Medeiros LE, Degrazia GA (2016) Contrasting structures between the decoupled and coupled states of the stable boundary layer. Q J R Meteorol Soc 142(695):693–702

Chamecki M, Dias NL, Freire LS (2018) A TKE-Based Framework for Studying Disturbed Atmospheric Surface Layer Flows and Application to Vertical Velocity Variance Over Canopies. Geophysical Research Letters 45:6734–6740, DOI 10.1029/2018GL077853

Falocchi M, Giovannini L, de Franceschi M, Zardi D (2019) A method to determine the characteristic time-scales of quasi-isotropic surface-layer turbulence over complex terrain: A case-study in the Adige Valley (Italian Alps). Q J R Meteorol Soc 145(719):495–512

Foken T, Wichura B (1996) Tools for quality assessment of surface-based flux measurements. Agricultural and forest meteorology 78(1-2):83–105

Grachev AA, Andreas EL, Fairall CW, Guest PS, Persson POG (2013) The Critical Richardson Number and Limits of Applicability of Local Similarity Theory in the Stable Boundary Layer. Boundary-Layer Meteorol 147:51–82

Højstrup J (1982) Velocity spectra in the unstable planetary boundary layer. J Atmos Sci 39(10):2239–2248

Howell JF, Mahrt L (1997) Multiresolution flux decomposition. Boundary-Layer Meteorol (83):117–137

Howell JF, Sun J (1999) Surface-layer fluxes in stable conditions. Boundary-Layer Meteorol (90):495–520

Kaimal JC, Finnigan JJ (1994) Atmospheric boundary layer flows. Their structure and measurement. Oxford University Press

Kaimal JC, Wyngaard JC, Izumi Y, Coté OR (1972) Spectral characteristics of surface-layer turbulence. Q J R Meteorol Soc 98:563–589

Mahrt L (2007) Weak-wind mesoscale meandering in the nocturnal boundary layer. Envirion Fluid Mech 7(4):331–347

Mahrt L (2014) Stably stratified atmospheric boundary layers. Annu Rev Fluid Mech 46:23–45, DOI 10.1146/annurev-fluid-010313-141354

Mahrt L, Vickers D (2002) Contrasting vertical structures of nocturnal boundary layers. Boundary-Layer Meteorol 105:351–363

Mahrt L, Thomas C, Richardson S, Seaman N, Stauffer DR, Zeeman M (2013) Non-stationary generation of weak turbulence for very stable and weak-wind conditions. Boundary-Layer Meteorol 147:179–199

Mahrt L, Sun J, Stauffer DR (2015) Dependence of Turbulent Velocities on Wind Speed and Stratification. Boundary-Layer Meteorol 155:55–71, DOI 10.1007/s10546-014-9992-5

Mazzola M, Tampieri F, Viola AP, Lanconelli C, Choi T (2016a) Stable boundary layer vertical scales in the Arctic: observations and analyses at Ny-Ålesund, Svalbard. Q J R Meteorol Soc pp 1250–1258, DOI 10.1002/qj.2727

Mazzola M, Viola AP, Lanconelli C, Vitale V (2016b) Atmospheric observations at the Amundsen-Nobile Climate Change Tower in Ny-Ålesund, Svalbard. Rendiconti Lincei 27(1):7–18

Mortarini L, Anfossi D (2015) Proposal of an empirical velocity spectrum formula in low-wind speed conditions. Q J R Meteorol Soc 141(686):85–97

Mortarini L, Cava D, Giostra U, Costa FD, Degrazia G, Anfossi D, Acevedo O (2019) Horizontal meandering as a distinctive feature of the stable boundary layer. J Atmos Sci (2019)

Schiavon M, Tampieri F, Bosveld F, Mazzola M, Castelli ST, Viola A, Yagüe C (2019) The Share of the Mean Turbulent Kinetic Energy in the Near-Neutral Surface Layer for High and Low Wind Speeds. Boundary-Layer Meteorol 172:81–106

Stiperski I, Calaf M (2018) Dependence of near-surface similarity scaling on the anisotropy of atmospheric turbulence. Q J R Meteorol Soc 144(712):641–657

Stiperski I, Calaf M, Rotach MW (2019) Scaling, anisotropy, and complexity in near-surface atmospheric turbulence. J Geophys Res: Atmos 124(3):1428–1448

Sun J, Mahrt L, Banta RM, Pichugina YL (2012) Turbulence regimes and turbulence intermittency in the stable boundary layer during cases-99. J Atmos Sci 69(1):338–351

Sun J, Lenschow DH, LeMone MA, Mahrt L (2016) The role of large-coherent-eddy transport in the atmospheric surface layer based on cases-99 observations. Boundary-Layer Meteorol 160(1):83–111

Tampieri F (2017) Turbulence and dispersion in the planetary boundary layer. Springer International

Tampieri F, Maurizi A, Viola A (2009) An investigation on temperature variance scaling in the atmospheric surface layer. Boundary-Layer Meteorol 132(1):31–42

Vickers D, Mahrt L (2003) The cospectral gap and turbulent flux calculations. J Atmos Ocean Technol 20:660–672

Vickers D, Mahrt L (2006) A solution for flux contamination by mesoscale motions with very weak turbulence. Boundary-Layer Meteorol 118(3):431–447

Van de Wiel B, Moene A, Jonker H, Baas P, Basu S, Donda J, Sun J, Holtslag A (2012) The minimum wind speed for sustainable turbulence in the nocturnal boundary layer. J Atmos Sci 69(11):3116–3127

Yadav AK, Raman S, Sharan M (1996) Surface layer turbulence spectra and dissipation rates during low winds in tropics. Boundary-Layer Meteorol 79(3):205–223

Zilitinkevich SS, Elperin T, Kleeorin N, Rogachevskii I, Esau IN (2013) A Hierarchy of Energy- and Flux-Budget (EFB) Turbulence Closure Models for Stably-Stratified Geophysical Flows. Boundary-Layer Meteorol 146:341–373